Measuring Parity Asymmetry of Gravitational Wave Backgrounds with a Heliocentric Detector Network in the mHz Band

Naoki Seto![ORCID]

Department of Physics, Kyoto University, Kyoto 606-8502, Japan

We discuss exploration for isotropic gravitational wave backgrounds around 1 mHz by correlation analysis, targeting both parity odd and even polarization modes. Even though the space interferometer LISA alone cannot probe the two modes due to cancellations, the outlook is being changed drastically by the strong development of other space detectors such as Taiji. In fact, a heliocentric interferometer network can hold a preferable geometrical symmetry illuminated by a virtual sphere off-center from the Sun. By utilizing an internal symmetry of data streams, we can optimally decompose the odd and even parity modes at the correlation analysis. By simultaneously using LISA and Taiji for ten years, our sensitivity to the two modes could reach $\sim 10^{-12}$ in terms of the normalized energy density.

Introduction.—Given the high penetration power of gravitational waves, a stochastic gravitational wave background could be a very important fossil from the early Universe for studying an extreme physical state [1,2]. For cosmology, we would like to primarily search for the monopole components of a background, since our observed Universe is nearly isotropic at large angular scale.

The Stokes V parameter characterizes the asymmetry between the amplitudes of the right- and left-handed polarized waves, and is proportional to $\Pi\Omega_{\rm GW}$ in the case of gravitational waves. Here, $\Omega_{\rm GW}$ is the normalized energy density and Π is the polarization degree ($\Pi = \pm1$ for 100% right- and left-handed waves). By measuring the V parameter, we can probe a parity violation process. Indeed, there are many cosmological arguments on the circularly polarized gravitational waves, including their potential roles for leptogenesis [3] and their production coupled with Chern-Simon terms during inflation (see, e.g., Ref. [4] for chromo-natural inflation, [5,6] for its extensions and [7] for a quantum gravity effect at a Lifshitz point) and phase transitions [8,9]. For example, depending on model parameters, due to a gauge field, a nearly 100% polarized ($|\Pi| \sim 1$) background might be generated above 10^{-11} Hz with the amplitude $\Omega_{\rm GW} \gtrsim 10^{-12}$ [5]. Therefore a detection of nonvanishing V parameter will have significant impacts on fundamental physics.

By correlating data streams of noise independent interferometers, we can directly measure the Stokes V parameter [10–12] (see also Refs. [13–15] for CMB analysis). For example, in the 10–1000 Hz band, using the current generation ground-based network for a few years, we will be able to detect the V parameter corresponding to $|\Pi|\Omega_{\rm GW} \sim 10^{-8}$ [11].

The band around 0.1m–1 Hz will be explored by space interferometers. The LISA project has a history of over 20 years [16,17], and its pathfinder mission recently had impressive success [18]. From its triangle constellation, we can generate multiple noise-independent data channels [19]. But, unfortunately, LISA is totally insensitive to the isotropic component of the V parameter, due to the exact cancellation resulting from the mirror symmetry at the interferometric plane [20]. With LISA alone, we can merely observe an anisotropic pattern (e.g., $l = 1$ and 3 harmonics) of the V parameter [20,21] (see also Ref. [22]). In fact, we also have an independent cancellation mechanism related to the symmetry of the data channels, and even the energy density $\Omega_{\rm GW}$ cannot be measured by correlating LISA's data streams (see also Refs. [1,23–25] for estimating $\Omega_{\rm GW}$ with the Sagnac modes). Future space plans such as big bang observer (BBO) and deci-hertz interferometer gravitational wave observatory (DECIGO) are designed to use multiple triangles for correlation analysis. By relatively tilting the orbits of two triangles, we can measure the even and odd parity modes down to $\Omega_{\rm GW} \sim \Omega_{\rm GW}|\Pi| \sim 10^{-16}$ [26], but these missions will be available much later than LISA.

However, nowadays, two other projects (TianQin [27] and Taiji [28]) are actively propelled in the mHz band, both aiming for operation around 2035, similar to LISA (see Fig. 1). Therefore, in the mHz band, we now have an increased chance to study an isotropic background by correlating LISA and Taiji and TainQin, without being hampered by the various signal cancellations. This Letter is the first quantitative study on this issue.

Since observation of a gravitational wave background is an intrinsically geometrical measurement, it is crucially important to see through the underlying symmetry of the network. From this standpoint, we limit our analysis to a network
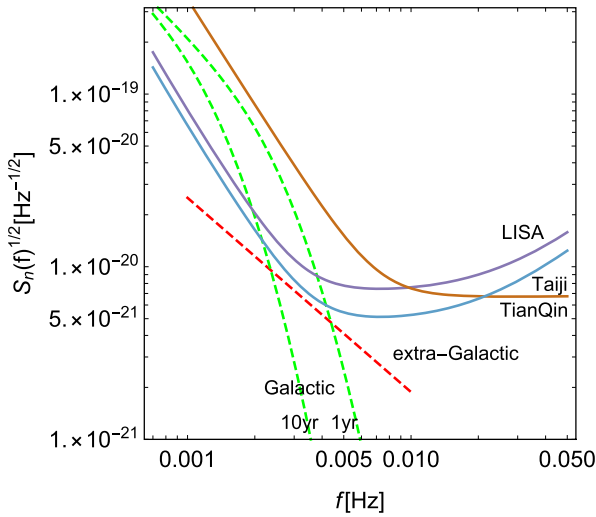
FIG. 1. Solid curves: the noise spectra of proposed space interferometers (LISA, Taiji and TianQin) for single data channels (A and E types). The green dashed curves are an estimation for the Galactic foreground (based on Ref. [29]) with observational time $T_{\rm obs} = 1$ and 10 yr. The red dashed curve shows the pessimistic model for extra-Galactic white dwarf confusion noise in [30] with $\Omega_{\rm GW}(f) \simeq 0.95 \times 10^{-12}(f/1~{\rm mHz})^{3/4}$ at 1 mHz–10 mHz.

composed by heliocentric interferometers (more specifically LISA and Taiji), paying special attention to the measurement of the two parity modes. In fact, a heliocentric network could have favorable geometrical symmetries that will allow us to easily make an optimal parity decomposition of a background.

Symmetries of the system.—Here, for a heliocentric detector network, we discuss two symmetries that are important for the parity decomposition. To the author's best knowledge, the first one has never been covered in the literature. The second one has been known (see, e.g., Ref. [31]), but can play a particularly interesting role when coupled with the first one.

Global symmetry: LISA has a heliocentric orbit moving 20° behind the Earth. Its three spacecrafts nearly keep a regular triangle with the arm length $L = 2.5 \times 10^6$ km [17]. This can be achieved by initially adding small eccentricities and inclinations to the spacecrafts, and the detector plane is resultantly inclined to the ecliptic plane by 60°. In Fig. 2, with the gray belt, we illustrate the envelope of the detector plane. The middle of the belt is on the ecliptic plane and corresponds to the orbital line of the barycenter of each triangle, with the radius $R_E = 1.5 \times 10^8$ km = 1.0 AU. The triangle is also spinning on the belt for a period of 1 yr (the so called cartwheel rotation).

Taiji moves 20° ahead of the Earth with its arm length $L = 3.0 \times 10^6$ km [28] (see also Ref. [32]), and shares the envelope with LISA (not opposite direction). The separation between LISA and Taiji is $D = 2R_E \sin(20°) = 1.0 \times 10^8$ km. TianQin has a geocentric orbit, and should be analyzed separately.
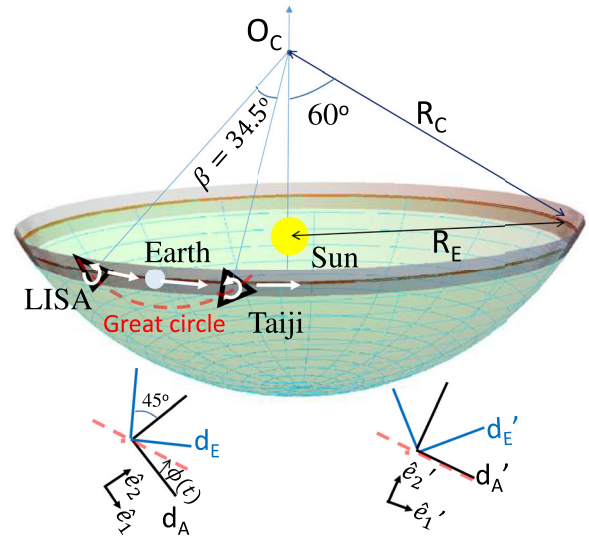

FIG. 2. Upper panel: the gray belt shows the envelope of the detector planes of the two heliocentric triangle interferometers, LISA and Taiji. The orange line is the orbital line of the barycenter of each triangle. The green surface is a part of the virtual sphere of radius $R_C = 1.15$ AU contacting the envelope belt. From the center O_C, the angular separation between LISA and Taiji is $\beta = 34.5°$ with the great circle shown with the dashed curve. The triangles spin on the belt (cartwheel motion). Lower left panel: the orientation of the detector tensors $\mathbf{d}_A$ and $\mathbf{d}_E$ that is attached to the LISA's triangle and characterized by the co-spinning orthonormal basis $(\hat{e}_1, \hat{e}_2)$. We define $\phi(t)$ for the time dependent miss-alignment angle relative to the great circle. Lower right panel: the orientation of the virtual detector tensors $\mathbf{d}'_A$ and $\mathbf{d}'_E$ associated with the aligned basis $(\hat{e}'_1, \hat{e}'_2)$. For the mirror transformation at the plane containing the great circle and O_C, we have $\hat{e}'_1 \to \hat{e}'_1$ and $\hat{e}'_2 \to -\hat{e}'_2$ (accordingly $\mathbf{d}'_A \to \mathbf{d}'_A$ and $\mathbf{d}'_E \to -\mathbf{d}'_E$).

Here, it should be noticed that the gray belt in Fig. 2 contacts with a sphere (hereafter "contact sphere") of radius $R_C = (\sqrt{3}/2)^{-1}R_E = 1.15$ AU. Interestingly, the contact sphere is not "heliocentric," but its center O_C is at 0.58 AU north of the ecliptic plane. As a sphere is a highly symmetric object and the search for gravitational wave backgrounds is a geometrical measurement, it would be advantageous to view the LISA-Taiji system in relation to the contact sphere. For example, from its center O_C, LISA and Taiji are separated by

$$\beta = 2\sin^{-1}[D/(2R_C)] = 34.5°. \qquad (1)$$

In order to quantify the relative orientation of LISA and Taiji interferometers on their detector planes (as discussed in the next subsection), we introduce a curve connecting the positions of the two observatories. Considering the existing symmetry of the system, the primary choice will be the great circle (geodesic) on the contact sphere, not the orbital line on the ecliptic plane.

Internal symmetry: Next we discuss symmetry within the triangle of the LISA constellation (essentially the same for Taiji). We can compose three interferometers at the three vertexes that are assumed to be equivalent (as in the standard literature) [19]. However, their data have correlated noises. Using the symmetry of the vertexes, we can make three noise independent data channels (A, E, T) as linear combinations of the three original data [19]. The Sagnac-like T channel has a negligible sensitivity to gravitational waves in the low frequency regime $f < c/(2\pi L) \sim 20$ mHz (with $L \ll D$), and can be used when measuring the instrumental noise level for the spectral estimation of a gravitational wave background [1,23–25]. For the correlation analysis, we thus consider using the A and E channels below, applying the low frequency approximation. Reflecting the original symmetry of the three vertexes, their noise spectra are identical [19], but, at the same time, using their correlation, we cannot measure the monopole pattern irrespective of the parity modes (see, e.g., Ref. [20]).

The A and E channels of LISA can be effectively regarded as responses of two L-shaped interferometers with orientation difference 45°, as shown in the lower left panel of Fig. 2 (see, e.g., Ref. [1]). They are attached to LISA's spinning triangle. Here, to characterize interferometric responses, we introduce the detector tensors $\mathbf{d}_A$ and $\mathbf{d}_E$. For the A channel, we have $\mathbf{d}_A = (\hat{e}_1 \otimes \hat{e}_1 - \hat{e}_2 \otimes \hat{e}_2)/2$ with the unit cospinning vectors $(\hat{e}_1, \hat{e}_2)$ for its two arm directions. For the E channel, using the same unit vectors, we have $\mathbf{d}_E = (\hat{e}_1 \otimes \hat{e}_2 + \hat{e}_2 \otimes \hat{e}_1)/2$. The combination $(\mathbf{d}_A, \mathbf{d}_E)$ forms the orthogonal basis for the detector tensors on the instantaneous detector plane. Note that the orientation of the detector tensors $\mathbf{d}_A$ and $\mathbf{d}_E$ are not aligned with the great circle (given the cartwheel spin rotation). We put the time-dependent misalignment angle by $\phi(t)$ as shown in Fig. 2.

Now we virtually rotate the basis $(\hat{e}_1, \hat{e}_2)$ commonly by the angle $\phi(t)$ so that $\hat{e}'_1$ is parallel to the great circle and respects the global symmetry of the network. We call the corresponding virtual detector tensors $\mathbf{d}_{A'} = (\hat{e}'_1 \otimes \hat{e}'_1 - \hat{e}'_2 \otimes \hat{e}'_2)/2$ and $\mathbf{d}_{E'} = (\hat{e}'_1 \otimes \hat{e}'_2 + \hat{e}'_2 \otimes \hat{e}'_1)/2$ (see the lower right panel in Fig. 2). By tensorial calculations, we can directly confirm the relation (e.g., Ref. [31])

$$\begin{pmatrix} \mathbf{d}_{A'} \\ \mathbf{d}_{E'} \end{pmatrix} = \begin{pmatrix} \cos 2\phi(t) & \sin 2\phi(t) \\ -\sin 2\phi(t) & \cos 2\phi(t) \end{pmatrix} \begin{pmatrix} \mathbf{d}_A \\ \mathbf{d}_E \end{pmatrix} \quad (2)$$

with the factor 2 reflecting the spin-2 nature. This means that, by linearly combining the LISA's original data channels A and E in the same manner as Eq. (2), we can actually obtain the data channels A' and E' whose detector tensors are the virtual ones $\mathbf{d}_{A'}$ and $\mathbf{d}_{E'}$. The new data set (A', E') has the same information content and noise spectrum as the original set (A, E), still without correlation (as easily confirmed). We can make a similar adjustment for Taiji.

We hereafter call the (virtually generated) aligned channels by (A_L, E_L) for the LISA and (A_T, E_T) for Taiji. In the next section, we consider the four interdetector combinations A_L-A_T, E_L-E_T, A_L-E_T, and E_L-A_T.

We should notice that, for the mirror transformation with respect to the plane containing the great circle and O_C, the unit vectors are transformed as $\hat{e}'_1 \to \hat{e}'_1$ and $\hat{e}'_2 \to -\hat{e}'_2$ both for LISA and Taiji (see the lower right panel in Fig. 2). Then the detector tensors have even parity for (A_L, A_T) and odd parity for (E_L, E_T) (see the definitions of $\mathbf{d}'_A$ and $\mathbf{d}'_E$ above). These properties would be essential for the optimal parity decomposition of a gravitational wave background.

Generally speaking, for two triangle detectors given at positions $\mathbf{p}_i$ ($i = 1, 2$) with associated normal vectors $\mathbf{n}_i$, the above symmetric mirror transformation can be applicable, only if the three vectors $\mathbf{p}_1$-$\mathbf{p}_2$, $\mathbf{n}_1$, and $\mathbf{n}_2$ are linearly dependent. In this sense, the gray envelope in Fig. 2 is geometrically special.

Gravitational wave background.—Monopole pattern: We use the Fourier decomposition of the metric perturbation induced by gravitational waves as

$$\mathbf{h}(t, \mathbf{x}) = \sum_{P=R,L} \int_{-\infty}^{\infty} df \int_{S^2} d\mathbf{n}\, h_P(f\mathbf{n}) \mathbf{e}^P(\mathbf{n}) e^{2\pi i f(\mathbf{n} \cdot \mathbf{x} - t)}, \quad (3)$$

where we adopted the right- and left-handed polarization bases $\mathbf{e}^{R,L}(\mathbf{n})$ with the unit propagation vector $\mathbf{n}$. They are given by the familiar linear polarization bases $\mathbf{e}^{+,\times}$ as

$$\mathbf{e}^R = (\mathbf{e}^+ + i\mathbf{e}^\times)/\sqrt{2}, \qquad \mathbf{e}^L = (\mathbf{e}^+ - i\mathbf{e}^\times)/\sqrt{2}. \quad (4)$$

Our target in this Letter is a stationary and isotropic gravitational wave background. For the monopole components, we can generally write [11,12,20]

$$\begin{pmatrix} \langle h_R(f\mathbf{n}) h_R(f'\mathbf{n}')^* \rangle \\ \langle h_L(f\mathbf{n}) h_L(f'\mathbf{n}')^* \rangle \end{pmatrix} = \frac{\delta_{\mathbf{n},\mathbf{n}'} \delta_{f,f'}}{8\pi} \begin{pmatrix} I(f) + V(f) \\ I(f) - V(f) \end{pmatrix} \quad (5)$$

with the Stokes parameters (I, V) and the Delta functions. In Eq. (5), the parameter I represents the total intensity of the background, while V characterizes the asymmetry between the right- and left-handed waves, as mentioned earlier. Note that, for the monopole mode, we do not have the Stokes Q and U parameters related to linear polarization.

Correlation analysis: In the Fourier space, reaction of an interferometer a (at $\mathbf{x} = \mathbf{x}_a$) to gravitational waves is given by

$$h_a(f) = \sum_{P=R,L} \int d\mathbf{n}\, h_P(f\mathbf{n})(\mathbf{d}_a : \mathbf{e}^P) e^{2\pi i f \mathbf{n} \cdot \mathbf{x}_a}. \quad (6)$$

Here the colon (:) represents the double contraction of the two tensors. Then correlation between two detectors a and b is given by $\langle h_a(f) h_b(f')^* \rangle = C_{ab}(f) \delta_{f,f'}$. Using Eqs. (4) and (5), we have

$$C_{ab}(f) = \frac{8\pi}{5}[\gamma_{Iab}(f)I(f) + \gamma_{Vab}(f)V(f)]. \quad (7)$$

Here γ_{Xab} are the overlap reduction functions $(X = I, V)$

$$\gamma_{Xab}(f) = \frac{5}{8\pi}\int d\boldsymbol{n} K_{Xab}(\boldsymbol{n})e^{2\pi i f \boldsymbol{n}\cdot(\boldsymbol{x}_a - \boldsymbol{x}_b)} \quad (8)$$

with the function $K_{Xab}(\boldsymbol{n})$ given by the beam patter functions $[F_a^{+,\times}(\boldsymbol{n}) \equiv \mathbf{d}_a : \mathbf{e}^{+,\times}(\boldsymbol{n})]$ as [11,20]

$$K_{Iab} = F_a^+ F_b^+ + F_a^\times F_b^\times, \quad K_{Vab} = -i(F_a^+ F_b^\times - F_a^\times F_b^+). \quad (9)$$

The overlap reduction functions describe the correlated responses of two interferometers to isotropic gravitational wave backgrounds. In Refs. [33,34], for ground based detectors, a simple analytic expression was derived for γ_{Iab}, fully using the symmetry of the earth surface as a sphere (similarly γ_{Vab} by Ref. [10]). Quite remarkably, for the LISA-Taiji system, by virtually introducing the contact sphere ($\sim 10^{4.5}$ times larger than the Earth), we can directly apply the simple expressions for γ_{Xab} originally provided for ground-based networks.

Moreover, the combinations made from the virtual data channels (A_L, E_L) and (A_T, E_T) are parity eigenstates for the mirror transformation mentioned at the end of the previous section. In concrete terms, A_L-A_T and E_L-E_T have even parity, and A_L-E_T and E_L-A_T have odd parity, corresponding to the special types classified in Ref. [11]. The even ones are sensitive only to the I mode (blind to V), and the odd ones are opposite. Accordingly, we can make perfect decompositions of the I and V modes, using the present pairs. For the overlap reduction functions, we can express

$$(\gamma_I(f), \gamma_V(f)) = (\Xi_1, 0) \quad \text{for } A_L\text{-}A_T,$$
$$(\gamma_I(f), \gamma_V(f)) = (\Xi_2, 0) \quad \text{for } E_L\text{-}E_T,$$
$$(\gamma_I(f), \gamma_V(f)) = (0, \Xi_3) \quad \text{for } A_L\text{-}E_T \quad \text{and} \quad E_L\text{-}A_T.$$

Here $\Xi_{1,2,3}$ depend on the opening angle β and $y \equiv 2\pi D f c^{-1}$ (D: LISA-Taiji distance). For example, we have [11]

$$\Xi_3(\beta, y) = \sin\frac{\beta}{2}\left[\left(-j_1 + \frac{7}{8}j_3\right) + \left(j_1 + \frac{3}{8}j_3\right)\cos\beta\right]. \quad (10)$$

with the spherical Bessel Functions $j_n(y)$ [11,33]. In Fig. 3, we present the overlap reduction functions in the low frequency regime. The period of the wavy profile is roughly given by $c/D \sim 3$ mHz, reflecting the spherical Bessel functions. The functions decay rapidly $\propto f^{-1}$ at $f \gg c/D$ as the phase coherence is lost by the positional difference. Below, we use simplified notations such as $\gamma_{IA_L E_T} = \gamma_{IAE}$.
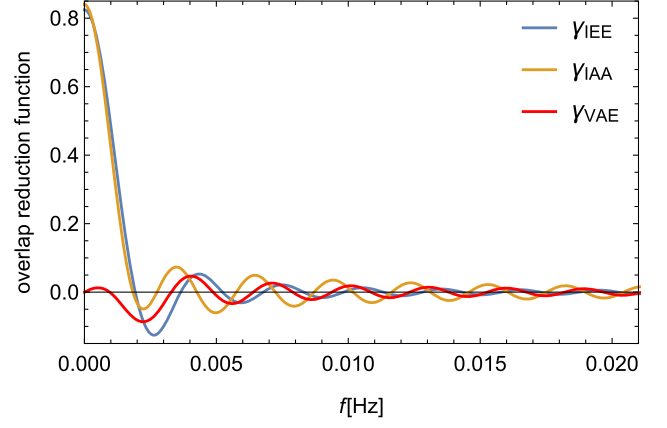

FIG. 3. The overlap reduction functions for the LISA-Taiji system. We can make a complete separation between I and V modes by pairing the data channels (A_L, E_L) and (A_T, E_T).

Detection prospects: Following the standard arguments on the correlation analysis [33,34], the signal-to-noise ratios SNR_X for two modes $(X = I, V)$ are given by

$$\text{SNR}_X^2 = \left(\frac{16\pi}{5}\right)^2 T_{\text{obs}}\left[2\int_{f_{\text{min}}}^{f_{\text{max}}} df \frac{\Gamma_X(f)X(f)^2}{f^6 S_L(f) S_T(f)}\right] \quad (11)$$

with $\Gamma_I = \gamma_{IAA}^2 + \gamma_{IEE}^2$ and $\Gamma_V = 2\gamma_{VAE}^2$ due to the optimal parity decomposition. Here T_{obs} is the observational period, $(f_{\text{min}}, f_{\text{max}})$ is the frequency range for signal integration, and $S_{L,T}(f)$ are the instrumental noise spectra of the two detectors (shown in Fig. 1) without including confusion noise in the present calculations.

For model characterization, we use the relations $[I(f), V(f)] = \rho_c/(4\pi^2 f^3)[\Omega_{\text{GW}}(f), \Pi(f)\Omega_{\text{GW}}(f)]$ with the critical density ρ_c. In Fig. 4, we present SNR_X $(X = I, V)$ respectively for the fiducial background $\Omega_{\text{GW}} = 10^{-11}$ and
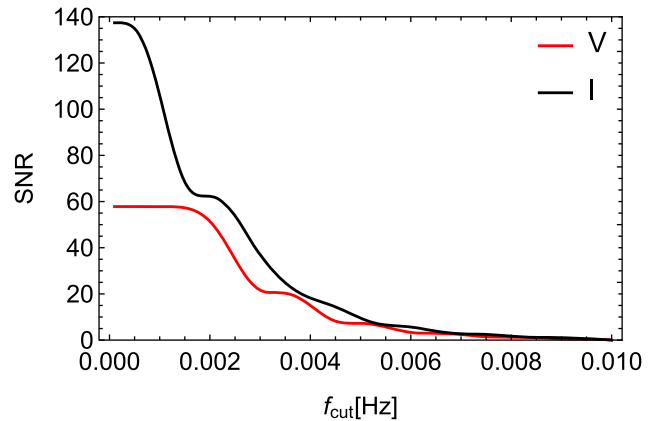

FIG. 4. Signal-to-noise ratios for the I and V mode searches as functions of the minimum frequency f_{min} for signal integration (with $f_{\text{max}} = 10$ mHz and $T_{\text{obs}} = 10$ yr). For signal models, we used $\Omega_{\text{GW}}(f) = 10^{-11}$ for the symmetric component and $\Pi(f)\Omega_{\text{GW}}(f) = 10^{-11}$ for the asymmetric one.

$\Pi\Omega_{\text{GW}} = 10^{-11}$ without f dependence. We put $T_{\text{obs}} = 10$ yr and $f_{\max} = 10$ mHz, but changed $f_{\min}$. For the numerical values in Fig. 4, we have simple scalings

$$\propto \left(\frac{\Omega_{\text{GW}}}{10^{-11}}\right)\left(\frac{T_{\text{obs}}}{10 \text{ yr}}\right)^{1/2}, \qquad \propto \left(\frac{\Omega_{\text{GW}}\Pi}{10^{-11}}\right)\left(\frac{T_{\text{obs}}}{10 \text{ yr}}\right)^{1/2}$$

for SNR_I and SNR_V. From these scaling relations, the detection limits ($\text{SNR}_X \sim 5$) are estimated to be $\Omega_{\text{GW}} \sim 10^{-12}$ and $\Pi\Omega_{\text{GW}} = 10^{-12}$ (for $f_{\min} = 2$ mHz and $T_{\text{obs}} = 10$ yr).

Interestingly, we can observe stairlike structures in Fig. 4, reflecting the shapes of the overlap reduction functions. For example, if we decrease $f_{\min}$ from 3 mHz to 2 mHz, SNR_V and SNR_I become 2.4 and 1.7 times larger. We will also have a significant increase of SNR_I by decreasing $f_{\min}$ further below 2 mHz, in contrast to SNR_V.

If we change $f_{\max}$ from 10 mHz to 30 mHz($> c/2\pi L$), keeping $f_{\min} = 2$ mHz, the numerical values SNR_V in Eq. (11) change less than 0.012% and 0.2%, respectively, for $\Omega_{\text{GW}}|\Pi| \propto f^0$ and f^1 (with similar corrections for SNR_I). In Eq. (11), this weak dependence on $f_{\max}$ is due to the factor f^{-6} and the suppression of the overlap reduction functions, and justifies our low frequency approximation for estimating $\text{SNR}_{I,V}$ (except for heavily blue-tilted spectra).

Discussion.—In this Letter, we discussed a correlation analysis for an isotropic gravitational wave background with heliocentric interferometers such as the LISA-Taiji network, paying special attention to the two parity modes and the underlying geometrical symmetries (see Fig. 2). Our analysis can be straightforwardly applied to a network composed by more than two heliocentric triangles detectors.

By correlating LISA and Taiji for ten years, our detection limit could reach $|\Pi|\Omega_{\text{GW}} \sim 10^{-12}$ that is 4 orders of magnitude better than the expected level with the current generation ground-based detector network in the near future. This is enough sensitivity for examining some of the theoretical predictions including chromo-natural inflation discussed in Ref. [5]. Owing to the clear parity decomposition, we might uncover a parity violation signature in a cosmological background, even if its energy density is dominated by astrophysical confusion noise.

As shown in Fig. 4, the estimated $\text{SNR}_{I,V}$ depend interestingly on the minimum frequency $f_{\min}$ for the signal integration. This frequency will be closely related to the processing status of the Galactic binary subtraction, and the observational time T_{obs} is the key strategic parameter (see Fig. 1). The foreground subtraction would be a crucial aspect for the follow-on space projects such as DECIGO and BBO targeting weak primordial background around 0.1–1 Hz [35,36] (see also Ref. [26] for potential orbital adjustment for the V parameter search). The correlation

analysis at mHz range would be useful also to examine the quality of the Galactic binary subtraction.

[1] J. D. Romano and N. J. Cornish, Living Rev. Relativity **20**, 2 (2017).

[2] C. Caprini and D. G. Figueroa, Classical Quantum Gravity **35**, 163001 (2018).

[3] S. H. S. Alexander, M. E. Peskin, and M. M. Sheikh-Jabbari, Phys. Rev. Lett. **96**, 081301 (2006).

[4] P. Adshead and M. Wyman, Phys. Rev. Lett. **108**, 261302 (2012).

[5] I. Obata, T. Miura, and J. Soda, Phys. Rev. D **92**, 063516 (2015).

[6] A. Maleknejad, M. Sheikh-Jabbari, and J. Soda, Phys. Rep. **528**, 161 (2013).

[7] T. Takahashi and J. Soda, Phys. Rev. Lett. **102**, 231301 (2009).

[8] T. Kahniashvili, G. Gogoberidze, and B. Ratra, Phys. Rev. Lett. **95**, 151301 (2005).

[9] J. Ellis, M. Fairbairn, M. Lewicki, V. Vaskonen, and A. Wickens, J. Cosmol. Astropart. Phys. 10 (2020) 032.

[10] N. Seto and A. Taruya, Phys. Rev. Lett. **99**, 121101 (2007).

[11] N. Seto and A. Taruya, Phys. Rev. D **77**, 103001 (2008).

[12] T. L. Smith and R. Caldwell, Phys. Rev. D **95**, 044036 (2017).

[13] A. Lue, L. M. Wang, and M. Kamionkowski, Phys. Rev. Lett. **83**, 1506 (1999).

[14] C. R. Contaldi, J. Magueijo, and L. Smolin, Phys. Rev. Lett. **101**, 141101 (2008).

[15] K. Inomata and M. Kamionkowski, Phys. Rev. Lett. **123**, 031305 (2019).

[16] P. L. Bender et al., LISA Pre-Phase A Report, 2nd ed. (Max Planck Institute for Quantum Optics, Garching, 1998).

[17] P. Amaro-Seoane et al., arXiv:1702.00786.

[18] M. Armano et al., Phys. Rev. Lett. **120**, 061101 (2018).

[19] T. A. Prince, M. Tinto, S. L. Larson, and J. W. Armstrong, Phys. Rev. D **66**, 122002 (2002).

[20] N. Seto, Phys. Rev. Lett. **97**, 151101 (2006).

[21] V. Domcke, J. Garcia-Bellido, M. Peloso, M. Pieroni, A. Ricciardone, L. Sorbo, and G. Tasinato, J. Cosmol. Astropart. Phys. 05 (2020) 028.

[22] E. Belgacem and M. Kamionkowski, Phys. Rev. D **102**, 023004 (2020).

[23] C. J. Hogan and P. L. Bender, Phys. Rev. D **64**, 062002 (2001).

[24] M. Tinto, J. M. Armstrong, and F. B. Estabrook, Classical Quantum Gravity **18**, 4081 (2001).

[25] M. R. Adams and N. J. Cornish, Phys. Rev. D **82**, 022002 (2010).

[26] N. Seto, Phys. Rev. D **75**, 061302(R) (2007).

[27] J. Luo et al., Classical Quantum Gravity **33**, 035010 (2016).

[28] W. R. Hu and Y. L. Wu, Natl. Sci. Rev. **4**, 685 (2017).

[29] T. Robson, N. J. Cornish, and C. Liu, Classical Quantum Gravity **36**, 105011 (2019).

[30] A. J. Farmer and E. Phinney, Mon. Not. R. Astron. Soc. **346,** 1197 (2003).

[31] N. Seto, Phys. Rev. D **69,** 123005 (2004).

[32] N. J. Cornish, Phys. Rev. D **65,** 022004 (2001).

[33] E. E. Flanagan, Phys. Rev. D **48,** 2389 (1993).

[34] B. Allen and J. D. Romano, Phys. Rev. D **59,** 102001 (1999).

[35] C. Cutler and J. Harms, Phys. Rev. D **73,** 042001 (2006).

[36] S. Kawamura *et al.*, Classical Quantum Gravity **23,** S125 (2006).